

High Frequency Gravitational Wave Bounds from Galactic Neutron Stars

V. Dandoy,^a T. Bertólez-Martínez,^b F. Costa.^c

^a*Service de Physique Theorique, C.P. 225, Université Libre de Bruxelles, Boulevard du Triomphe, B-1050 Brussels, Belgium*

^b*Departament de Física Quàntica i Astrofísica and Institut de Ciències del Cosmos, Universitat de Barcelona, Diagonal 647, E-08028 Barcelona, Spain*

^c*Institute for Theoretical Physics, Georg-August University Göttingen, Friedrich-Hund-Platz 1, Göttingen, D-37077 Germany*

E-mail: virgile.dandoy@ulb.be, antoni.bertolez@fqa.ub.edu, francesco.costa@theorie.physik.uni-goettingen.de

ABSTRACT: High-Frequency Gravitational Waves (HFGWs) constitute a unique window on the early Universe as well as exotic astrophysical objects. While the current gravitational wave experiments are more dedicated to the low frequency regime, the graviton conversion into photons in a strong magnetic field constitutes a powerful tool to probe HFGWs. In this paper, we show that neutron stars, due to their extreme magnetic field, are a perfect laboratory to study the conversion of HFGWs into photons. Using realistic models for the galactic neutron star population, we calculate for the first time the expected photon flux induced by the conversion of an isotropic stochastic gravitational wave background in the magnetosphere of the ensemble of neutron stars present in the Milky Way. We compare this photon flux to the observed one from several telescopes and derive upper limits on the stochastic gravitational wave background in the frequency range 10^8 Hz - 10^{25} Hz. We find our limits to be competitive in the frequency range 10^8 Hz - 10^{12} Hz.

Contents

1	Introduction	1
2	Graviton-Photon Conversion in Neutron Stars	3
2.1	Radial Trajectory	5
2.2	Generic Trajectory	7
3	Photon Flux from GW Conversion in Galactic Neutron Stars	8
3.1	Upper Limits	11
4	Conclusion	12
A	Neutron Star Distribution	13

1 Introduction

The search for low-frequency (nHz-kHz) Gravitational Waves (GWs) has been strongly motivated by theoretical predictions in the last decades. This has naturally led to a series of experimental projects aiming to detect GWs below the \sim kHz. Among them, the Laser Interferometer Gravitational-Wave Observatory (LIGO) [1] first observed GWs in the kHz range from binary black holes. More recently, the Pulsar Timing Array (PTA) community (NANOGrav [2], PPTA [3], EPTA [4], and IPTA [5]) has claimed strong evidence of a Stochastic Gravitational Wave Background (SGWB) in the nHz regime. The latter is strongly motivated by supermassive black holes binaries [6, 7]. Early Universe sources have been shown to offer a similar level of explanation to the SGWB [8–19].

In analogy to the electromagnetic spectrum that covers orders of magnitudes in frequency, GWs could be produced over a large frequency range, each of them being associated with different physical phenomena. Interestingly, GWs with frequencies larger than the ones currently searched for in experiments are difficult to motivate with known astrophysical objects or standard cosmology [20]. Any detection of such GWs would, therefore, be a hint for exotic early Universe sources; phase transitions, preheating after inflation, oscillons, cosmic strings, or exotic astrophysical objects, for instance, primordial black holes [21–33] (see Ref. [34] for a review of different sources). These primordial GWs are expected to propagate freely in the Universe to form a SGWB, as in the case of the background potentially observed by the PTA.

However, High-Frequency Gravitational Waves (HFGWs) have been significantly less explored than the low-frequency range. The main reason for this relies on the fact that GW detectors are usually sensitive to GWs with wavelengths comparable to their size. Targeting HFGWs, therefore, requires a radically different experimental setup (see Refs. [20, 35–40]

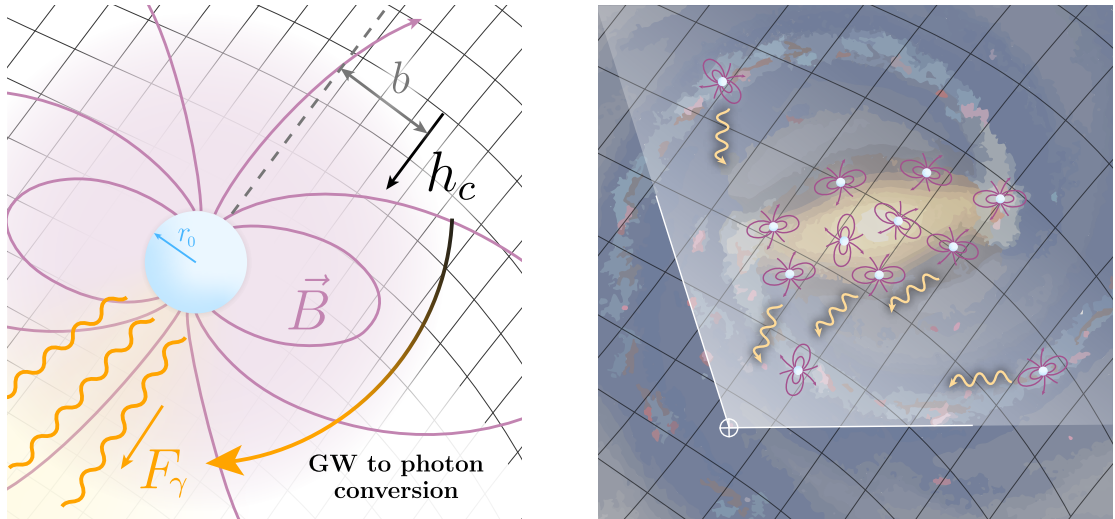


Figure 1: GWs with a characteristic strain h_c can be converted into a flux of photons F_γ inside a neutron star magnetic field \vec{B} , through the so-called inverse Gertsenshtein effect. Here, b is the impact factor of the graviton trajectory. The whole population of neutron stars inside the galaxy produces a photon flux on top of the known galactic emission from the graviton-photon conversion of a SWGB.

for a non-exhaustive list of recent proposals).

Nonetheless, the detection of HFGWs may be possible via the (inverse) Gertsenshtein effect [41, 42]: similarly to axions, GWs in the presence of a magnetic field can convert into photons. This has naturally led to use the existing axion experiments as HFGW detectors and translating the existing constraints on the axion to photon coupling into constraints on the GWs abundance Ω_{gw} (usually expressed in terms of the characteristic strain h_c) [43–47], see Fig. 6.

More recently, the conversion of a high-frequency SGWB into photons in astrophysical environments has been considered. For instance, Refs. [48, 49] studied the impact on the CMB/X-ray measurements of the conversion of MHz-GHz GWs in the cosmic magnetic field and extracted strong constraints on the GWs abundance. Similar conversion has been studied in the magnetosphere of solar system planets [50] and the Crab/Gemini pulsars [51], as well as in the geomagnetic field, and the galactic and intergalactic magnetic fields [52, 53].

One of the main reasons that makes astrophysical environments particularly suitable for observing the Gertsenshtein effect lies in the natural presence of strong magnetic fields (which enhance the graviton-photon conversion) impossible to produce in the laboratory. Among the most extreme examples, neutron stars (NSs) are known to possess a surface magnetic field around $B \approx 10^{13}$ Gauss [54, 55] and, therefore, appear to be one of the most efficient places to convert gravitons into photons. Furthermore, NS magnetospheres are relatively well understood and allow for reliable predictions. In the presence of a SWGB the ensemble of NSs present in the Milky Way—estimated to be around 10^9 NSs [56, 57]—would then induce a photon flux at the same frequency as the SGWB, as illustrated in Fig. 1.

The galactic NS population therefore behaves as a powerful tool to probe the presence of a high frequency SGWB.

Motivated by the last statement, we calculate in this work the radiated photon flux from the conversion of a high frequency SGWB in the magnetosphere of the ensemble of NSs within the Milky Way (see Ref. [58] for a similar study in the axion case). Using recent models for the NS magnetic field, spin period, and spatial distribution [54, 55], we compare this photon flux to the observations conducted by several telescopes (see Ref. [59] for a summary). Finally we extract competitive constraints on the amount of GWs in a large frequency range, from $\sim 10^8$ Hz to $\sim 10^{25}$ Hz.

In the following, we first start in Sec. 2 by recalling the inverse Gertsenshtein effect in the specific context of NS magnetospheres. We describe in Sec. 3 the expected induced photon flux from the galactic NSs and detail the method used to extract constraints on the GW abundance. Finally, we show our results in Sec. 3.1 and conclude in Sec. 4. The specific models for the NS distributions are discussed in App. A.

2 Graviton-Photon Conversion in Neutron Stars

The GW-to-photons conversion is described by the inverse Gertsenshtein effect which is the result of the coupling between gravity and electromagnetism via the Lagrangian term $\mathcal{L} \supset F_{\mu\nu}F^{\mu\nu} = g^{\rho\mu}g^{\sigma\nu}F_{\rho\sigma}F_{\mu\nu}$. Note that we are working in natural units and using the $\eta_{\mu\nu} = \text{diag}(1, -1, -1, -1)$ metric signature. Considering the GW (and then the photons) propagating in a direction perpendicular to the magnetic field, one can derive the leading order equation of motion for the gravitons and photons polarizations. Assuming a homogeneous magnetic field, that reads [41, 50]

$$\left(\omega - i\partial_n + \begin{pmatrix} \Delta_{\perp} & \Delta_M & \Delta_R & 0 \\ \Delta_M & 0 & 0 & 0 \\ \Delta_R & 0 & \Delta_{\parallel} & \Delta_M \\ 0 & 0 & \Delta_M & 0 \end{pmatrix} \right) \begin{pmatrix} A_{\perp} \\ h_+ \\ A_{\parallel} \\ h_{\times} \end{pmatrix} = 0. \quad (2.1)$$

The GW polarizations are h_{\times} and h_+ , while A_{\parallel} and A_{\perp} are respectively the parallel and perpendicular photon polarizations to the magnetic field. As we will discuss in the following, we approximate the GW to be transverse to the magnetic field \vec{B} . Defining B_t as the component transverse to the direction of motion of the incoming GW, and \vec{e}_t as the unit vector in this transverse direction, then this means that the longitudinal component $\vec{B} - B_t\vec{e}_t$ is negligible. Since Δ_R is proportional to this longitudinal component, then we can assume $\Delta_R \approx 0$ and treat Eq. (2.1) as two independent equations of motion [50, 53] that read

$$\left(\omega - i\partial_n + \begin{pmatrix} \Delta_{\parallel(\perp)} & \Delta_M \\ \Delta_M & 0 \end{pmatrix} \right) \begin{pmatrix} A_{\parallel(\perp)} \\ h_{\times(+)} \end{pmatrix} = 0. \quad (2.2)$$

Notice that $\times(+)$ GW polarizations will be converted into $\parallel(\perp)$ photon polarizations. The graviton-photon mixing is $\Delta_M = \frac{1}{2}\kappa B_t$ with $\kappa = (16\pi G)^{1/2}$. In the presence of the external

magnetic field B_t , an effective mass $\Delta_{\parallel(\perp)}$ is induced for the photons,

$$\Delta_{\parallel(\perp)} = \Delta_{\text{pla},\parallel(\perp)} + \Delta_{\text{vac},\parallel(\perp)} \quad (2.3)$$

Each term describes a different physical effect: $\Delta_{\text{pla},\parallel} = -\frac{m_{\text{pla}}^2}{2\omega}$ and $\Delta_{\text{pla},\perp} = -\frac{m_{\text{pla}}^2 \omega^2}{2\omega(\omega^2 - \omega_c^2)}$ are the plasma corrections to the photon mass, with $\omega_c \approx 10^{19} \left(\frac{B}{10^{12}\text{G}}\right)$ Hz [41]. The difference between the two polarizations comes from the Cotton-Mouton effect [51, 60, 61]. $\Delta_{\text{vac},\parallel(\perp)} = 7(4) \frac{\alpha\omega}{90\pi} \left(\frac{B_t}{B_c}\right)^2$ is the QED vacuum correction. We defined $m_{\text{pla}}^2 = \frac{4\pi\alpha n_c}{m_c}$, $B_c = \frac{m_e^2}{e}$ and $\omega = 2\pi f$, with f the graviton/photon frequency. Moreover, α and e are the QED fine structure constant and the electron charge. Finally, n_c and m_c are the number density and invariant mass of the particles in the plasma. In NSs we have $n_c \approx n_e$ and $m_c \approx m_e$, the electron number density and the electron mass, respectively.

In NSs, the magnetic field is not homogeneous. Still, the previous system of equation can be solved perturbatively in the case of an inhomogeneous magnetic field (see Ref. [41]). With this, the total GW-photon conversion probability can be extracted for the \parallel (\perp) polarization and is given by [41, 62]

$$P_{\parallel(\perp)}(f) = \left| \int_{\ell_0}^{\ell_1} d\ell \Delta_{\text{M}}(\ell) \exp \left\{ -i \int_{\ell_0}^{\ell} d\ell' \Delta_{\parallel(\perp)}(\ell') \right\} \right|^2, \quad (2.4)$$

considering a generic GW path in the magnetic field between ℓ_0 and ℓ_1 ¹.

In the specific case of NSs, the magnetic field extends from its surface r_0 to the end of the magnetosphere $R \approx T/(2\pi)$ [51], with T the rotation period. Assuming equipartition and averaging over the directions of the magnetic field we parametrize the component of the magnetic field perpendicular to the GW trajectory in the NS magnetosphere as [51]

$$B_t = \sqrt{\frac{2}{3}} B_0 \left(\frac{r}{r_0}\right)^{-3}, \quad (2.5)$$

where B_0 is the magnetic field at the NS surface, r the distance to the NS center and r_0 the radius of the NS. We consider the magnetic field as a dipole aligned with the rotation axis. This leads to a reliable upper bound on the GW strain, since a dipole provides the minimum amount of GW-photon conversion.

Finally, the electron number density n_e in the magnetosphere can be described in a Goldreich-Julian model [51, 63]

$$n_e(r) = 7 \times 10^{-2} \left(\frac{1\text{s}}{T}\right) \left(\frac{B_t(r)}{1\text{G}}\right) \text{cm}^{-3}. \quad (2.6)$$

In what follows we first derive an analytic expression for the conversion probability of gravitons with radial trajectories inside the magnetosphere, and then we compute it for arbitrary trajectories.

¹In what follows, we assume that the typical wavelength of the GW is much smaller than the NS magnetosphere. This, in addition to the large occupation number, allows us to describe GWs as made of individual gravitons with defined trajectories. A more precise study of the problem using a wave description of the system is left for future works.

2.1 Radial Trajectory

For radial trajectories throughout the magnetosphere, the gravitons would propagate from r_0 to R . Since all relevant quantities are spherically symmetric, Eq. (2.1) simply becomes

$$P_{0,\parallel(\perp)}(f) = 2 \left| \int_{r_0}^R dr \Delta_M(r) \exp \left\{ -i \int_{r_0}^r dr' \Delta_{\parallel(\perp)}(r') \right\} \right|^2, \quad (2.7)$$

where the factor 2 arises since the graviton is actually traveling twice along this path (once when entering the magnetosphere and once when exiting it).

While this integral will be solved numerically in the next sections, we derive here analytical expressions in the limit of high and low frequencies. To this point, we choose as the upper limit of the integral $R \rightarrow \infty$. In fact, the magnetic field decays cubically with the distance and the unphysical contribution outside the magnetosphere is negligible.

Let us start with the parallel polarization. Since $\Delta_{\text{pla},\parallel}$ and $\Delta_{\text{vac},\parallel}$ scale as $1/f$ and f respectively, we have that at high frequencies we can approximate $\Delta_{\parallel} \approx \Delta_{\text{vac},\parallel}$ and low frequencies $\Delta_{\parallel} \approx \Delta_{\text{pla},\parallel}$. Thus, at high frequencies

$$P_{0,\parallel}^{\text{high-}f} \approx \frac{2(\Delta_M(r_0)r_0)^2}{5^{6/5}(\Delta_{\text{vac},\parallel}(r_0)r_0)^{4/5}} \left| \Gamma\left(\frac{2}{5}\right) - \Gamma\left(\frac{2}{5}, -\frac{i\Delta_{\text{vac},\parallel}(r_0)r_0}{5}\right) \right|^2,$$

where $\Gamma(x, y)$ is the incomplete Gamma function. Similar expression has been derived for instance in Ref.[50].

At low frequencies,

$$P_{0,\parallel}^{\text{low-}f} \approx \frac{2\Delta_M^2(r_0)}{\Delta_{\text{pla},\parallel}^2(r_0)} \left| \exp\left(\frac{i\Delta_{\text{pla},\parallel}(r_0)r_0}{2}\right) - 1 \right|^2. \quad (2.8)$$

The high (low) frequency regime is defined for frequencies in general much higher (lower) than the transition frequency. The transition frequency can be found by $|\Delta_{\text{pla},\parallel}| \approx |\Delta_{\text{vac},\parallel}|$,

$$f_{\text{tra}} \approx 6.5 \times \frac{m_e^{3/2}}{e} \sqrt{\frac{2\pi}{B_0 T}}. \quad (2.9)$$

For frequencies around f_{tra} , there is a region where $\Delta_{\text{pla},\parallel}$ and $\Delta_{\text{vac},\parallel}$ compensate, and thus the photon effective mass vanishes. This region is close to the NS surface. When this mass is small enough, the graviton-photon conversion satisfies both momentum and energy conservation and is enhanced. The maximum of the conversion probability would therefore be around f_{tra} . A good approximation of the maximum conversion probability is given by

$$P_{0,\parallel}^{\text{max}} \approx P_{0,\parallel}^{\text{high-}f}(f_{\text{tra}}). \quad (2.10)$$

In contrast, for much larger (smaller) frequencies, the effective photon mass provided by $\Delta_{\text{vac},\parallel}$ ($\Delta_{\text{pla},\parallel}$) decreases significantly the conversion probability²³.

²In practice, for much larger frequencies than f_{tra} there is still a region where $\Delta_{\text{pla},\parallel}$ and $\Delta_{\text{vac},\parallel}$ compensate. However, as the frequency increases, this one is pushed to larger radius and is suppressed by the decaying magnetic field.

³This is actually a general statement: the larger the effective mass, the lower the conversion probability.

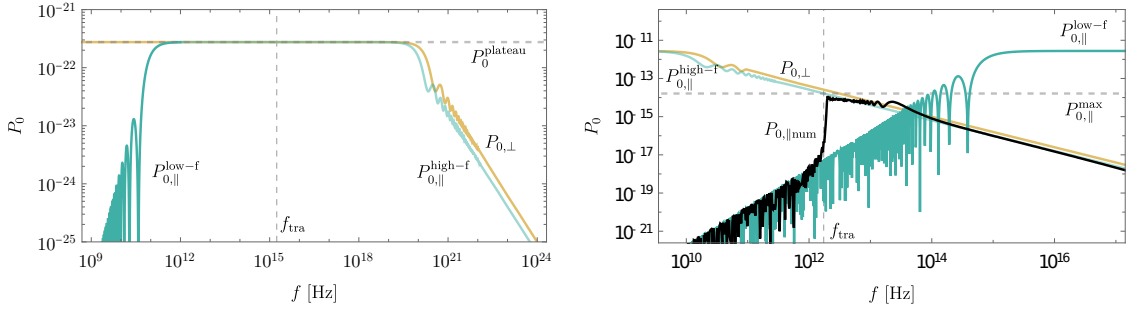


Figure 2: Conversion probability as a function of the frequency for an NS with $B_0 = 10^8$ Gauss, $T = 0.1$ s, and $r_0 = 10$ km (left) and for $B_0 = 10^{13}$ Gauss, $T = 1$ s, and $r_0 = 10$ km (right). The curves respectively in dark and light green are the analytical approximation at low frequencies and high frequencies for the parallel polarization. The yellow curve is the analytical approximation for the perpendicular polarization which matches the numerical result. The dashed gray line is the maximum conversion probability approximation for the parallel polarization and the black dashed line is f_{tra} . Finally, the black curve in the right panel is the numerical result for the parallel polarization.

For the perpendicular polarization, we notice that in the typical NS magnetic fields $\Delta_{pla,\perp} \approx 0$ due to a $\omega_c \approx 10^{19} \left(\frac{B}{10^{12}\text{G}}\right)$ Hz suppression. This means that $\Delta_{\perp} \approx \Delta_{vac,\perp}$ and we have a continuation of the high-frequency behavior as described in Eq. (2.8) even at low frequencies. The perpendicular polarization conversion probability is simply given by Eq. (2.8) with $\Delta_{vac,\parallel}(r_0) \rightarrow \Delta_{vac,\perp}(r_0)$. As we will see, this will induce that at low frequencies gravitons with $+$ polarization have a much higher chance of being converted into \parallel photons, as opposed to \times gravitons.

In Fig. 2 we present the analytical results in dark green (high-frequency) and light green (low-frequency) for the parallel polarizations and in yellow for the perpendicular one. The left(right) panel corresponds to a surface magnetic field of 10^8 (10^{13}) Gauss. For the \parallel polarization, we find good agreements with the numerical solution of Eq. (2.7) (black curve in the right panel) for frequencies much larger and much smaller than f_{tra} . For frequencies around f_{tra} , the conversion probability is enhanced due to a region on the path of the graviton where $\Delta_{pla,\parallel}$ and $\Delta_{vac,\parallel}$ compensate. We denote by $P_{0,\parallel}^{\max}$ the maximum conversion probability for the \parallel polarization. Since the plasma(vacuum) effect scales as $\sim 1/f$ ($\sim f$), at lower(larger) frequencies the effective mass increases significantly. From the same arguments, it explains why the conversion probability drops quickly in these regions. For the \perp polarization, the conversion probability is simply given by Eq. (2.8) (replacing $\Delta_{vac,\parallel}$ by $\Delta_{vac,\perp}$). Since $\Delta_{vac,\perp} \sim f$, the effective photon becomes smaller as we lower the frequency. Therefore, the conversion probability increases as the frequency gets lower, until it reaches a maximum when the effective mass becomes negligible. The numerical results match the analytical approximation.

2.2 Generic Trajectory

Most gravitons crossing the magnetosphere are not radial, but have a linear trajectory with a particular impact parameter b , as shown in Fig. 1. Such path can be parametrized if we align the y axis to the graviton trajectory, and thus Eq. (2.1) becomes

$$P_{\parallel(\perp)}(f, b) = 2 \left| \int_{y_{\min}}^{y_{\max}} dy \Delta_M(y) \exp \left\{ -i \int_{y_{\min}}^y dy' \Delta_{\parallel(\perp)}(y') \right\} \right|^2. \quad (2.11)$$

Here $y_{\max} = \sqrt{R^2 - b^2}$ and $y_{\min} = 0$ if $b > r_0$ (the graviton is not crossing the NS) and $y_{\min} = \sqrt{r_0^2 - b^2}$ if $b < r_0$ (the graviton is crossing the NS). Similarly to the radial trajectory, the factor 2 arises from symmetry.

We can gain some intuition on what this probability should look like. We have seen in the previous section that the conversion is efficient when the effective photon mass is small (i.e. $\Delta_{\parallel(\perp)} \approx 0$). Since \vec{B} decays as $1/r^3$, $\Delta_{\parallel(\perp)}$ also decreases as the radius increases. Thus, for each frequency, there exists a radius further from which gravitons can convert efficiently. However, this “sweet” conversion spot does not extend much further because Δ_M drops quickly too. Hence due to the necessity of having both a large magnetic field and a small photon mass, the efficient conversion region is limited to a thin shell of critical radius $b_c(f)$ right after the effective photon mass becomes negligible.

As long as the graviton crosses this shell (i.e. $b < b_c(f)$), the probability of conversion remains constant, since this contribution strongly dominates the integral (2.11). In particular, it matches the probability calculated in the previous section: $P_{0,\parallel(\perp)}(f)$. If the impact parameter b becomes large enough so that the graviton does not cross the shell (i.e. $b > b_c(f)$), then we should expect for the conversion probability to be suppressed due to the decaying magnetic field. In particular, an analytical computation shows a $1/b^4$ suppression on the probability.

A numerical result for the probability (2.11) as a function of b is shown in the left panel of Fig. 3. In the right panel, we show the critical impact parameter $b_c(f)$. Since the photon effective mass depends on both the magnetic field and the polarization, so does $b_c(f)$. We make this explicit by writing $b_{c,\parallel}(f, B_0)$ and $b_{c,\perp}(f, B_0)$. They differ as follows:

- For the \parallel polarization, the effective photon mass is given by $\Delta_{\text{vac},\parallel} + \Delta_{\text{pla},\parallel}$. Since $\Delta_{\text{pla},\parallel} \propto 1/f$, the \parallel polarization has a larger effective photon mass at small frequencies. Therefore, the critical impact parameter $b_{c,\parallel}(f, B_0)$ increases at low f .
- For the \perp polarization, $\Delta_{\text{vac},\perp}$ is suppressed at small frequencies, and thus $b_{c,\perp}(f)$ decreases with f .

Finally, the effective photon mass grows with the surface magnetic field B_0 , so $b_c(f)$ increases with it too.

In what will follow, we consider that, for a given frequency, only gravitons with $b < b_{c,\parallel(\perp)}(f, B_0)$ are converted. For those gravitons the conversion probability is the one calculated under the radial approximation. Explicitly,

$$P_{\parallel(\perp)}(f, b, B_0) \approx \begin{cases} P_{0,\parallel(\perp)}(f, B_0) & \text{if } b < b_{c,\parallel(\perp)}(f, B_0) \\ 0 & \text{if } b > b_{c,\parallel(\perp)}(f, B_0) \end{cases}. \quad (2.12)$$

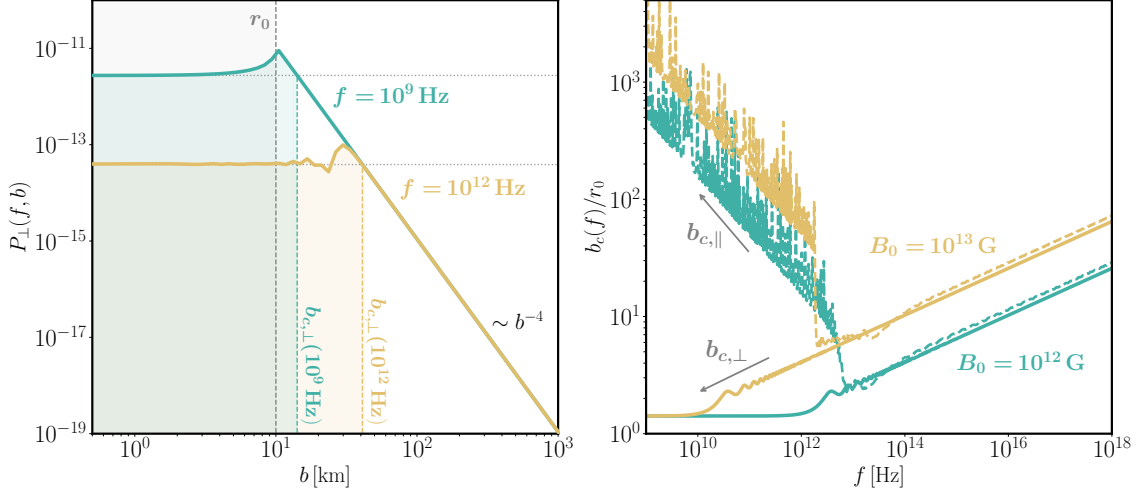


Figure 3: *Left:* Conversion probability for the perpendicular polarization as a function of the impact parameter. Green and yellow lines show the probability for $f = 10^9$ Hz and $f = 10^{12}$ Hz, respectively. Vertical and horizontal dashed lines show the value of $b_c(f)$ and P_0^{plateau} for each frequency, respectively. The magnetic field is set to $B_0 = 10^{13}$ G. *Right:* Critical impact parameter as a function of the frequency. Green and yellow lines show $B_0 = 10^{12}$ G and $B_0 = 10^{13}$ G, respectively. Solid and dashed lines show the perpendicular and parallel polarizations, respectively. In both plots, the NS spin period and radius has been taken to be $T = 1$ s, and $r_0 = 10$ km.

3 Photon Flux from GW Conversion in Galactic Neutron Stars

As we have just seen, the magnetosphere of NSs is an interesting region for conversion of GWs to photons. Then, a diffuse and isotropic flux of HFGWs would be converted into a galactic photon flux, which would be strongly correlated with the galactic NS distribution. In this section we use the conversion probability just derived to compute the total photon flux from the conversion of a HFGW background on each of the NSs of the galaxy.

An isotropic stochastic GW background carries a flux of gravitons F_{gw} which can be written in terms of its spectral energy density $d\rho_{\text{gw}}/df$ as [52]

$$\frac{\partial F_{\text{gw}}}{\partial f \partial \Omega} = \frac{1}{4\pi} \frac{d\rho_{\text{gw}}}{df}, \quad (3.1)$$

where Ω is the solid angle. It follows that the outgoing flux of gravitons is

$$\frac{\partial F_{\text{gw}}}{\partial f} = \pi^2 M_{\text{pl}}^2 f h_c^2, \quad (3.2)$$

where M_{pl} is the reduced Planck mass, and we have integrated over half a sphere. We have introduced the characteristic strain h_c [64],

$$\frac{d\rho_{\text{gw}}}{df} = 2\pi^2 h_c^2 M_{\text{pl}}^2 f. \quad (3.3)$$

Gravitons convert only if they cross the magnetosphere with an impact parameter $b < b_{\parallel(\perp)}(f, B_0)$. Then, the induced photon flux, F_γ , received on Earth is

$$\frac{\partial F_\gamma}{\partial f} = \pi^2 M_{\text{pl}}^2 f h_c^2 \left[\left(\frac{b_{c,\parallel}(f, B_0)}{r} \right)^2 P_{0,\parallel}(f) + \left(\frac{b_{c,\perp}(f, B_0)}{r} \right)^2 P_{0,\perp}(f) \right], \quad (3.4)$$

where r is the distance of the NS to Earth.

NSs are distributed in the galaxy following a distribution $n_{\text{ns}}(\mathbf{r})$. Since the conversion probability (2.11) depends on the NS magnetic field B_0 and rotation period T , we also need their distribution among galactic NSs. With respect to these, the galactic NS population is divided into two main subgroups: active and dead stars. While the former can emit a coherent radio pulsed emission and are detectable, the latter have already lost too much spin through such emission and are not detectable anymore. Thus, dead NSs have, in general, a longer period. Still, both have an active magnetosphere and must be taken into account (see App. A).

From NS observations, different models for their evolution and properties have been developed. We choose two of them [54, 55], which differ in the evolution of the magnetic field. While [54] has a constant magnetic field, [55] accounts for its decay and predicts a weaker magnetosphere for dead NS. Although both models are consistent with data (see for instance Refs. [65, 66]), the former leads to stronger constraints and the latter to more conservative ones. We keep both in order to illustrate the sensitivity of our predictions to the models, which is the dominant uncertainty of our results. Then, each model predicts a different distribution for both variables. Independently of the model, the probability distribution for both variables inside of each subgroup is well represented by a log-normal distribution, and so we distinguish $P_{\text{act.}}(B_0, T)$ for active NSs from $P_{\text{dead}}(B_0, T)$ for dead NSs. It is estimated that 0.4% of the galactic NS population are active, while 99.6% are dead [58]. Further details on the spatial and probability distributions can be found in App. A.

All in all, the total induced photon flux from the galactic NSs, $F_\gamma^{\text{galac.}}$, can be obtained by integrating over the whole galactic NS distributions,

$$\begin{aligned} \frac{\partial F_\gamma^{\text{galac.}}}{\partial f}(f, h_c) = & \int d^3\mathbf{r} n_{\text{ns}}(\mathbf{r}) \int dB_0 dT \left(0.004 \times P_{\text{act.}}(B_0, T) \right. \\ & \left. + 0.996 \times P_{\text{dead}}(B_0, T) \right) \frac{\partial F_\gamma}{\partial f}(B_0, T, \mathbf{r}, f, h_c). \end{aligned} \quad (3.5)$$

In Fig. 4 (left), we plot the frequency dependence of this flux, normalised as $h_c^{-2} f \partial F_\gamma^{\text{galac.}} / \partial f$. Since $F_\gamma^{\text{galac.}}(f, h_c) \propto h_c^2$, this is a quantity independent of the characteristic strain. At large frequencies this quantity increases as $f^{7/5}$. The flux keeps growing with the frequency since the amount of GWs for a fixed value of h_c increases as $d\rho_{\text{gw}}/df \propto f$ while the conversion probability decays slower.

In Fig. 5, we show an illustrative example of the all sky flux map from a SGWB characterized by a characteristic strain $h_c = 10^{-25}$ at frequency $f = 10^{15}$ Hz, following the model with constant magnetic field. The model with decaying magnetic field predicts a $\mathcal{O}(0.001)$

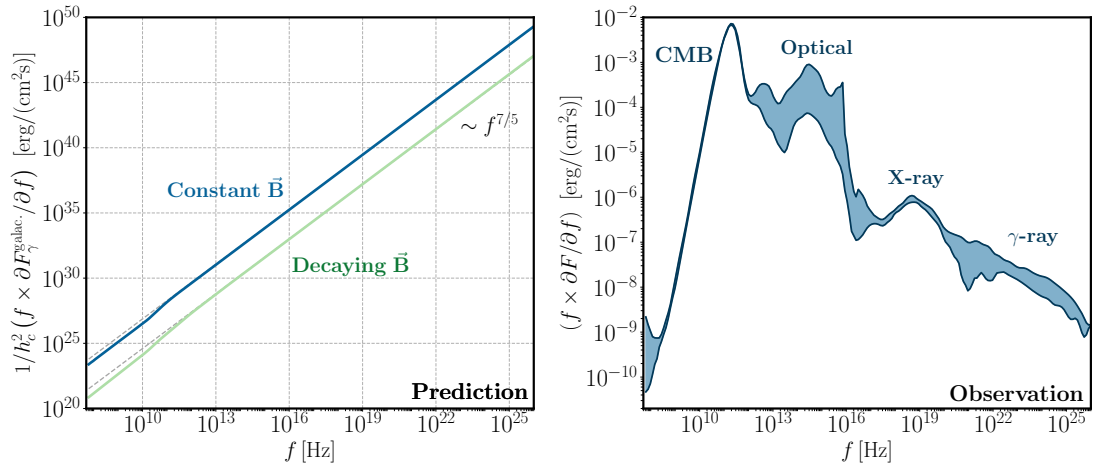


Figure 4: *Left:* Predicted frequency spectrum of the total induced flux $\partial F_\gamma^{\text{galac.}}/\partial f$, normalized by $1/h_c^2$. Blue and green lines show the results for a NS model with constant and decaying \vec{B} , respectively. We set $r_0 = 10$ km. *Right:* Frequency spectrum measured on Earth, adapted from Ref. [59]. The thick band corresponds to the 95% confidence interval. Data allows to put a bound on h_c at each frequency.

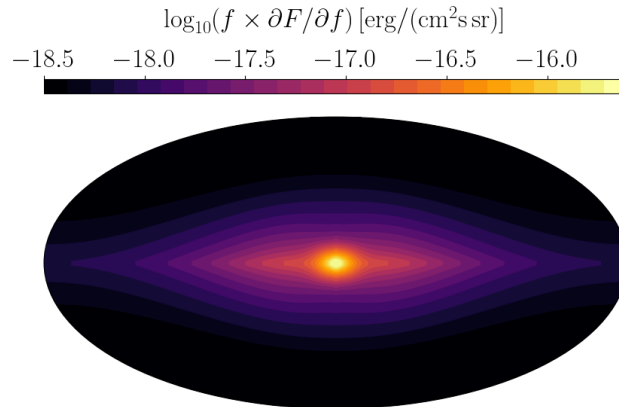


Figure 5: All sky map of the induced photon flux from the conversion of an isotropic SGWB with $h_c = 10^{-25}$ and frequency $f = 10^{15}$ Hz. We considered a population of NSs with constant magnetic field. When considering the case of a decaying magnetic field, similar angular distribution is expected with a flux reduced by a factor $\mathcal{O}(10^{-3})$.

weaker flux. Since the latter predicts a lower surface magnetic fields (see App. A), less gravitons would be converted in the NS magnetospheres. For this reason, the flux from the decaying magnetic field model is typically smaller.

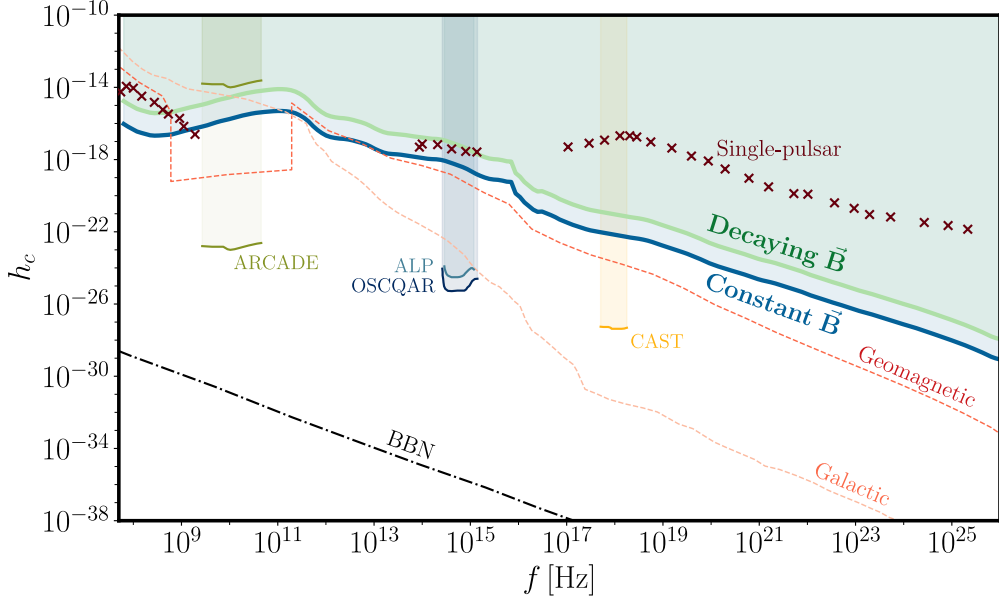


Figure 6: Constraints on the characteristic strain h_c from different experiments. Blue and green solid lines represent our bounds from an induced photon flux in the magnetosphere of the galactic NSs, for NS models with a constant and decaying \vec{B} , respectively. We also show limits from OSQAR, ALP and CAST [44] as well as the one from ARCADE (the upper and lower lines corresponding to uncertainty on the cosmic magnetic field) [49] and Big Bang Nucleosynthesis [67] (black dashed-dotted lines). The red and orange dashed curves represent the limits from conversion in the geomagnetic field and galactic magnetic field respectively [53]. Finally, the red crosses are the constraints from the Crab pulsar observation [51]. The code and data to reproduce this figure are publicly available [\[51\]](#).

3.1 Upper Limits

The photon flux from this SGWB conversion must now be compared to observations of the all-sky integrated flux. In Fig. 4 (right) we show the latter after the subtraction of all galactic sources which are known and accounted for [59]. Then, $F_\gamma^{\text{galac.}}(f, h_c)$ can not be brighter than this flux, otherwise it would be in conflict with current observations. Thus, we can place an upper bound on the characteristic strain h_c by demanding that our flux does not exceed the cosmic radiation background reported by various experiments.

The limits found with this method are reported as blue and green solid lines in Fig. 6, for a constant and a decaying magnetic field, respectively. For comparison, we also show the current limits derived from axion experiments: OSQAR, ALP and CAST [44] as well as those derived using ARCADE [49] (see Refs.[20, 68] for a summary of those constraints). The orange and red dashed curves show the upper limits derived when comparing the induced photon-flux produced in the geomagnetic field and galactic magnetic field [53] to the same telescope observations used in this work. Interestingly, we find our limits to be the best in the frequency range ($10^8 - 10^9$) Hz and comparable to the geomagnetic bounds around ($10^{12} - 10^{15}$) Hz. In contrast with bounds from geomagnetic conversion, our re-

sults predict a flux which peaks in the Galactic Center, as shown in Fig. 5. Observations of the galactic flux angular distribution or focused on the Galactic Center could improve our bounds with respect to others. At larger frequencies, the induced photon flux from galactic NSs is systematically smaller than the one from the geomagnetic field and galactic magnetic field. For this reason our limits are less competitive at large frequencies.

Comparable calculations to the ones presented in this work have been also performed in the case of the Crab pulsar, with data obtained from single-pulsar observations. In Ref. [51], the induced photon-flux has been compared to the current observations of this NS and led to the red crosses in Fig. 6. At least for present data, using the galactic population of NSs at large frequencies increases by several orders of magnitudes the constraints compared to a single pulsar analysis.

Finally, the black dashed-dotted line shows the upper limit on the amount of gravitational waves produced before Big Bang Nucleosynthesis (BBN), which would contribute to the number of relativistic degrees of freedom [67]. Since this limit does not apply to post-BBN or monochromatic sources, current bounds are important even if they fall short compared to BBN constraints. Still, these bounds correspond to GWs with $d\Omega_{\text{gw}}/d\log f \gg 1$. Such sources would need to be extremely monochromatic in order not to overclose the Universe. Even if they emitted in a more reasonable frequency width, no known cosmological sources can produce HFGWs intense enough to saturate our bounds. The mergers of exotic compact objects or cosmological sources could produce GWs with the right frequency, but with $\Omega_{\text{gw}} < 1$ [20, 49, 69–71]. Therefore, further improvement is still required for all state-of-the-art HFGWs analysis to constrain such sources.

With respect to our results, the bounds here presented will be improved by more precise all-sky observations. It might also be possible to profit from the accumulation of neutron stars in the Galactic center direction. However, such backgrounds are harder to model and a lower signal-to-noise ratio would make an improvement challenging.

Again, these kind of analysis would only constrain homogeneous fluxes, either of cosmological or astrophysical (but distributed around all the sky) origin. Single localized events would require a perfect alignment between the NS and the GW source and require a different approach to an all-sky observation. Thus, these are beyond the scope of our work.

4 Conclusion

In this paper we presented upper limits on the high frequency SGWB from the (inverse) Gertsenshtein effect in the magnetosphere of the galactic NSs. This is particularly important since this region of the GW spectrum is only partially constrained and may be used to probe new physics phenomena.

As a first step, we recalled the graviton-photon conversion in the NS magnetosphere. An effective conversion can only happen in regions where the effective photon mass is low enough so that both energy and momentum are conserved in the process. Due to the Cotton-Mouton effect, the photon polarization perpendicular to the external magnetic field is less massive compared to the parallel one which translates into a significantly larger conversion of the + polarized gravitons compared to the \times ones (as also observed by [51]).

For both polarizations, we derived analytical formulae for the conversion probability. From this, we extracted the induced photon flux from a single NS and then from the ensemble of galactic NSs using two realistic population models [54, 55]. The first assumes a decaying magnetic field whereas the second considers a constant surface magnetic field over time. Since the graviton-photon conversion is enhanced by large magnetic fields, we find that the second model predicts a larger induced photon flux. Finally, we compared this induced photon flux to several telescope observations. Asking that the flux does not exceed the current observations provides upper limits on the SGWB.

Our conclusions are the following: first, since many phenomena could induce a SGWB, it is highly expected for the galactic NSs to be an important site of graviton-photon conversion. However, only a large-enough high frequency SGWB would induce a photon signal which can be potentially detectable with future experiments. Such SGWB could be explained by mergers of light primordial black holes. Secondly, we derived competitive upper limits in the frequency range $\sim (10^8 - 10^{15})$ Hz, confirming, and improving in some frequency range, the existing constraints from similar studies on the geomagnetic and galactic magnetic field [49, 53]. Beyond $\sim 10^{15}$ Hz, we found the induced photon flux from galactic NSs to be significantly smaller than the one from the galactic magnetic field [53]. This naturally translates into weaker constraints.

Acknowledgements

We thank Valerie Domcke, Jordi Salvadó and Jinsu Kim for useful comments on the manuscript and Nicolas Grimbaum, Asuka Ito, Kazunori Kohri, Kazunori Nakayama for useful discussion. TB acknowledges financial support from the Spanish grants PID2022-136224NB-C21, PID2019-108122GBC32, PID2019-105614GB-C21, and from the State Agency for Research of the Spanish Ministry of Science and Innovation through the “Unit of Excellence María de Maeztu 2020-2023” award to the Institute of Cosmos Sciences (CEX2019-000918-M). The work of F.C. is supported by the European Union’s Horizon 2020 research and innovation programme under the Marie Skłodowska-Curie grant agreement No 860881-HIDDeN.

A Neutron Star Distribution

To accurately predict the total induced photon flux on Earth, a realistic distribution for the properties of the NSs must be used (surface magnetic field B ⁴ and spin period T).

Numerous NS observations have been performed (more than 2000 rotation-powered NSs [65, 66]). Based on those, recent efforts have been made in developing NS models (initial magnetic field and period distributions as well as their time evolution) capable of reproducing the observed data. In this appendix, we summarized the ideas of two distinct models that are used in the main text [54, 55].

In the first (Model 1, referred to in the main text as “constant magnetic field”), the NS magnetic field is assumed constant and therefore fixed to its initial birth value. On the

⁴Later on, B will always refer to the surface magnetic field.

Initial Distributions		
Model	Variance [G], [s]	Mean [G], [s]
Model 1	$\sigma_B = 0.55, \sigma_T = 0.15$	$\mu_B = 12.95, \mu_T = 0.3$
Model 2	$\sigma_B = 0.6, \sigma_T = 0.1$	$\mu_B = 13.25, \mu_T = 0.25$

Table 1: Variance and mean values of the log-normal distributions (A.6) for the initial surface magnetic field B_0 and spin period T_0 as derived in Refs.[54, 55].

other hand, the spin period increases in time as the NS loses energy by dipole radiation and plasma effects (see Refs.[72–74]). It is found that the period evolves as [58]

$$T(t) = T_0 \sqrt{1 + \frac{4t}{3\tau_0}}, \quad (\text{A.1})$$

with

$$\tau_0 \sim 10^4 \left(\frac{10^{12}\text{G}}{B} \right)^2 \left(\frac{T_0}{0.01\text{s}} \right)^2 \text{ yr}, \quad (\text{A.2})$$

where T_0 is the initial spin period and B the constant magnetic field of the NS.

Eventually, as the period increases, the NS spin might be low enough to prevent a coherent radio-pulsed emission. At this stage, the NS becomes undetectable (further on referred to as "dead" or "inactive" NSs, although it is important to stress that it does not imply that it loses its magnetic field) [75]. This transition is expected to happen when the ratio B/T^2 is smaller than [76]

$$B/T^2 < 0.34 \times 10^{12} \text{G s}^{-2}. \quad (\text{A.3})$$

Post-death, NSs are expected to lose energy only through dipole radiation [58], this translates into a modified period evolution,

$$T(t > t_{\text{death}}) = T(t_{\text{death}}) \sqrt{1 + \tan^2 \alpha \left(1 - e^{-\frac{4(t-t_{\text{death}})\cos^2 \alpha}{3\tau_0}} \right)}, \quad (\text{A.4})$$

where t_{death} is the time at which the NS becomes inactive and α is the misalignment angle between the NS rotation and magnetic axis (see ref.[58]).

In the second model (Model 2, referred in the main text as "decaying magnetic field"), the spin period time evolution is considered to be the same as in Model 1. Nonetheless, the magnetic field is here considered decaying in time. This is the essential difference between these two models. For the magnetic field decay, we follow Ref.[58] and describe the time evolution of the surface magnetic field as

$$\frac{dB}{dt} = -B \left(\frac{1}{\tau_{\text{Ohm}}} + \left(\frac{B}{B_0} \right)^2 \frac{1}{\tau_{\text{Ambip}}} \right), \quad (\text{A.5})$$

where B_0 is the initial magnetic field and $\tau_{\text{Ambip}}, \tau_{\text{Ohm}}$ are the decay rate of the magnetic field by ambipolar effects [77, 78] and ohmic dissipation [79], respectively.

In Refs.[54, 55, 58], a large population of NSs have been simulated and evolved until today using the two above models. In order to reproduce the observational data [65, 66], the initial distributions for the surface magnetic field B_0 and period T_0 have been found to be given by,

$$\begin{aligned} P(B_0) &= \frac{1}{\sqrt{2\pi} B_0 \sigma_B} \exp \left[-\frac{\log^2(B_0/\mu_B)}{(2\sigma_B^2)} \right], \\ P(T_0) &= \frac{1}{\sqrt{2\pi} T_0 \sigma_T} \exp \left[-\frac{\log^2(T_0/\mu_T)}{(2\sigma_T^2)} \right], \end{aligned} \tag{A.6}$$

where (σ_B, μ_B) and (σ_T, μ_T) are given for Model 1 and Model 2 in Tab.1. Furthermore, from the same simulations, the today's magnetic field and period distributions can be extracted. In both models, it has been found that only $\sim 0.4\%$ of the NSs are still active [58]. In Fig.7, we show today's distributions for both the surface magnetic field and the spin period in the two models. In particular, we show separately the distributions (normalized) for the active and dead NSs. It can be appreciated that, in both models, the dead NSs have larger periods. This is directly related to the fact that dead NSs have more time to evolve their spin period to larger values. On the right panel, the magnetic field distributions for the active and dead NSs in Model 1 are relatively similar with slightly larger values for the dead NSs. This is due to the fact that for larger magnetic fields, τ_0 gets smaller making the spin period decrease faster. Interestingly, the magnetic field distributions for the Model 2 are quite different. Recalling that in this model, the magnetic field is assumed to decay in time, the dead NSs, assumed to be older than the active ones, have more time to decay and for this reason, their surface magnetic field is significantly reduced compared to the active population (assumed younger).

There exist different methods to determine the number of neutron stars in the Milky Way. On the one hand, supernovae explosions, which lead into to NS, release an important amount of iron. The study of the chemical composition of the galaxy in the Milky Way and its iron content suggests that about 10^9 NSs have been produced [80]. On the other hand, the disk stellar birth rate has been observed to be approximately constant over the galactic history [81]. This implies a roughly constant NS formation rate as well, which leads to 4×10^8 NSs in the disk. The stellar population in the bulge is expected to have formed in a much shorter time scale around 12 Gyrs ago, and its stellar mass function is skewed toward high masses [82]. The early time population of heavy stars led to a more important NS population in the bulge, around 6×10^8 [56]. All in all, this leads again to the estimation of 10^9 NSs in the galaxy. We follow standard choices in the literature and take $N_{\text{bulge}} = 4.8 \times 10^8$ and $N_{\text{disk}} = 3.2 \times 10^8$ NSs [56, 57]. Of course, depending of the total number of NSs, the upper limits derived in this work would change. It is expected that increasing (decreasing) the number of NSs would translate into stronger (weaker) constraints.

Each population follows a different spatial distribution. The disk distribution (in a frame with the origin at the galactic center) has been extracted from millisecond pulsar observa-

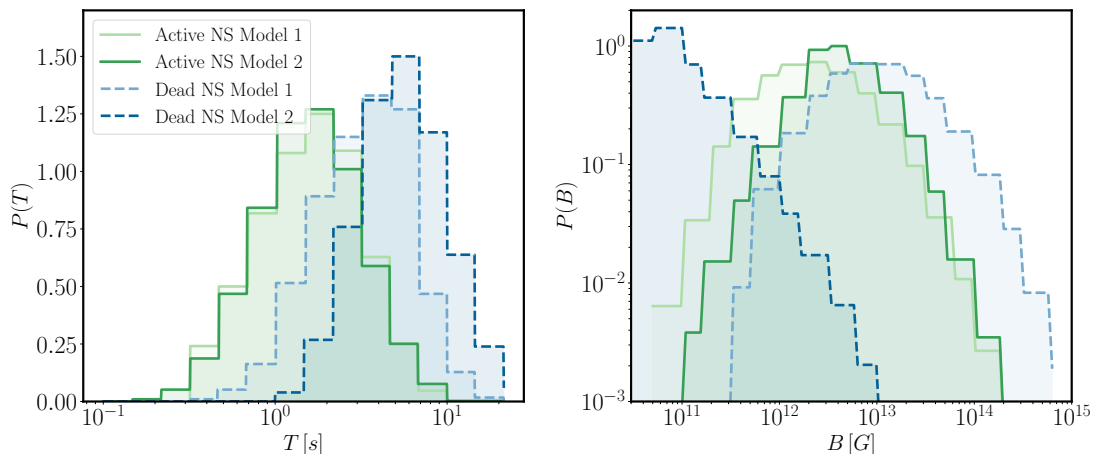


Figure 7: *Left:* Today’s distribution for the spin period T of the active (green) and dead (blue) NSs. Model 1 and Model 2 are represented by the light and dark colors respectively. *Right:* Same for the surface magnetic field B . In both cases, the distributions are normalized so that $\int d\log(x)P(x) = 1$. This figure is adapted from Fig.4 of Ref.[58].

tions [83, 84] (see also [85] for another parametrisation),

$$n_{\text{disk}}(r, z) = N_{\text{disk}} \frac{C^{B+2} e^{-C}}{4\pi r_{\odot}^2 \sigma_z \Gamma(B+2)} \left(\frac{r}{r_{\odot}}\right)^B e^{-C \frac{r-r_{\odot}}{r_{\odot}}} e^{-|z|/\sigma_z}, \quad (\text{A.7})$$

where $B = 3.91$, $C = 7.54$, $\sigma_z = 0.76 \text{ kpc}$ and r_{\odot} is the sun distance from the galactic center. The bulge distribution is taken from Ref. [86] and is assumed to follow the stellar distribution [87, 88],

$$n_{\text{bulge}}(r, z) = N_{\text{bulge}} \frac{11.1}{\text{kpc}^3} \frac{e^{-(r'/r_{\text{cut}})^2}}{(1+r'/r_0)^{\lambda}}, \quad (\text{A.8})$$

with $r' = \sqrt{r^2 + (z/0.5)^2}$, $r_0 = 0.075 \text{ kpc}$, $\lambda = 1.8$ and $r_{\text{cut}} = 2.1 \text{ kpc}$.

As already mentioned, from this spatial distribution, 0.4% will be active NSs with surface magnetic field and spin period distributed as in Fig.7 (green solid lines) and 99.6% will be inactive NSs with surface magnetic field and spin period distributed as the blue dashed lines in Fig.7. In the main text, the total flux on Earth from graviton-to-photon conversion in the NS magnetospheres has been calculated for both Model 1 and Model 2. For both models, we assumed an NS radius of $r_0 = 10 \text{ km}$ REF.

References

- [1] **LIGO Scientific, Virgo**, B. P. Abbott et al., *Observation of Gravitational Waves from a Binary Black Hole Merger*, *Phys. Rev. Lett.* **116** (2016), no. 6 061102, [1602.03837].
- [2] **NANOGrav**, G. Agazie et al., *The NANOGrav 15 yr Data Set: Evidence for a Gravitational-wave Background*, *Astrophys. J. Lett.* **951** (2023), no. 1 L8, [2306.16213].

- [3] D. J. Reardon et al., *Search for an Isotropic Gravitational-wave Background with the Parkes Pulsar Timing Array*, *Astrophys. J. Lett.* **951** (2023), no. 1 L6, [2306.16215].
- [4] **EPTA, InPTA:**, J. Antoniadis et al., *The second data release from the European Pulsar Timing Array - III. Search for gravitational wave signals*, *Astron. Astrophys.* **678** (2023) A50, [2306.16214].
- [5] J. Antoniadis et al., *The International Pulsar Timing Array second data release: Search for an isotropic gravitational wave background*, *Mon. Not. Roy. Astron. Soc.* **510** (2022), no. 4 4873–4887, [2201.03980].
- [6] H. Middleton, A. Sesana, S. Chen, A. Vecchio, W. Del Pozzo, et al., *Retracted: Correction to: Massive black hole binary systems and the NANOGrav 12.5 yr results*, *Mon. Not. Roy. Astron. Soc.* **502** (2021), no. 1 L99–L103, [2011.01246]. [Erratum: *Mon. Not. Roy. Astron. Soc.* 526, L34 (2023)].
- [7] E. S. Phinney, *A Practical theorem on gravitational wave backgrounds*, [astro-ph/0108028](https://arxiv.org/abs/astro-ph/0108028).
- [8] S. Vagnozzi, *Implications of the NANOGrav results for inflation*, *Mon. Not. Roy. Astron. Soc.* **502** (2021), no. 1 L11–L15, [2009.13432].
- [9] Z.-C. Chen, Y.-M. Wu, and Q.-G. Huang, *Searching for isotropic stochastic gravitational-wave background in the international pulsar timing array second data release*, *Commun. Theor. Phys.* **74** (2022), no. 10 105402, [2109.00296].
- [10] A. S. Sakharov, Y. N. Eroshenko, and S. G. Rubin, *Looking at the NANOGrav signal through the anthropic window of axionlike particles*, *Phys. Rev. D* **104** (2021), no. 4 043005, [2104.08750].
- [11] M. Benetti, L. L. Graef, and S. Vagnozzi, *Primordial gravitational waves from NANOGrav: A broken power-law approach*, *Phys. Rev. D* **105** (2022), no. 4 043520, [2111.04758].
- [12] A. Ashoorioon, K. Reza zadeh, and A. Rostami, *NANOGrav signal from the end of inflation and the LIGO mass and heavier primordial black holes*, *Phys. Lett. B* **835** (2022) 137542, [2202.01131].
- [13] Y.-M. Wu, Z.-C. Chen, and Q.-G. Huang, *Search for stochastic gravitational-wave background from massive gravity in the NANOGrav 12.5-year dataset*, *Phys. Rev. D* **107** (2023), no. 4 042003, [2302.00229].
- [14] **IPTA**, M. Falxa et al., *Searching for continuous Gravitational Waves in the second data release of the International Pulsar Timing Array*, *Mon. Not. Roy. Astron. Soc.* **521** (2023), no. 4 5077–5086, [2303.10767].
- [15] Y.-M. Wu, Z.-C. Chen, and Q.-G. Huang, *Pulsar timing residual induced by ultralight tensor dark matter*, *JCAP* **09** (2023) 021, [2305.08091].
- [16] V. Dandoy, V. Domcke, and F. Rompineve, *Search for scalar induced gravitational waves in the international pulsar timing array data release 2 and NANOgrav 12.5 years datasets*, *SciPost Phys. Core* **6** (2023) 060, [2302.07901].
- [17] E. Madge, E. Morgante, C. Puchades-Ibáñez, N. Ramberg, W. Ratzinger, et al., *Primordial gravitational waves in the nano-Hertz regime and PTA data — towards solving the GW inverse problem*, *JHEP* **10** (2023) 171, [2306.14856].
- [18] S. Kawai and J. Kim, *Probing the inflationary moduli space with gravitational waves*, *Phys. Rev. D* **108** (2023), no. 10 103537, [2308.13272].

- [19] S. Vagnozzi, *Inflationary interpretation of the stochastic gravitational wave background signal detected by pulsar timing array experiments*, *JHEAp* **39** (2023) 81–98, [[2306.16912](#)].
- [20] N. Aggarwal et al., *Challenges and opportunities of gravitational-wave searches at MHz to GHz frequencies*, *Living Rev. Rel.* **24** (2021), no. 1 4, [[2011.12414](#)].
- [21] J. Ghiglieri and M. Laine, *Gravitational wave background from Standard Model physics: Qualitative features*, *JCAP* **07** (2015) 022, [[1504.02569](#)].
- [22] S. Wang, T. Terada, and K. Kohri, *Prospective constraints on the primordial black hole abundance from the stochastic gravitational-wave backgrounds produced by coalescing events and curvature perturbations*, *Phys. Rev. D* **99** (2019), no. 10 103531, [[1903.05924](#)]. [Erratum: *Phys.Rev.D* 101, 069901 (2020)].
- [23] J. Ghiglieri, G. Jackson, M. Laine, and Y. Zhu, *Gravitational wave background from Standard Model physics: Complete leading order*, *JHEP* **07** (2020) 092, [[2004.11392](#)].
- [24] J. Ghiglieri, J. Schütte-Engel, and E. Speranza, *Freezing-In Gravitational Waves*, [2211.16513](#).
- [25] S. Y. Khlebnikov and I. I. Tkachev, *Relic gravitational waves produced after preheating*, *Phys. Rev. D* **56** (1997) 653–660, [[hep-ph/9701423](#)].
- [26] R. Easther and E. A. Lim, *Stochastic gravitational wave production after inflation*, *JCAP* **04** (2006) 010, [[astro-ph/0601617](#)].
- [27] J. Garcia-Bellido and D. G. Figueroa, *A stochastic background of gravitational waves from hybrid preheating*, *Phys. Rev. Lett.* **98** (2007) 061302, [[astro-ph/0701014](#)].
- [28] R. Anantua, R. Easther, and J. T. Giblin, *GUT-Scale Primordial Black Holes: Consequences and Constraints*, *Phys. Rev. Lett.* **103** (2009) 111303, [[0812.0825](#)].
- [29] A. D. Dolgov and D. Ejlli, *Relic gravitational waves from light primordial black holes*, *Phys. Rev. D* **84** (2011) 024028, [[1105.2303](#)].
- [30] R. Dong, W. H. Kinney, and D. Stojkovic, *Gravitational wave production by Hawking radiation from rotating primordial black holes*, *JCAP* **10** (2016) 034, [[1511.05642](#)].
- [31] F. Costa, S. Khan, and J. Kim, *A two-component vector WIMP — fermion FIMP dark matter model with an extended seesaw mechanism*, *JHEP* **12** (2022) 165, [[2209.13653](#)].
- [32] F. Costa, S. Khan, and J. Kim, *A two-component dark matter model and its associated gravitational waves*, *JHEP* **06** (2022) 026, [[2202.13126](#)].
- [33] T. C. Gehrman, B. Shams Es Haghi, K. Sinha, and T. Xu, *The primordial black holes that disappeared: connections to dark matter and MHz-GHz gravitational Waves*, *JCAP* **10** (2023) 001, [[2304.09194](#)].
- [34] C. Caprini and D. G. Figueroa, *Cosmological Backgrounds of Gravitational Waves*, *Class. Quant. Grav.* **35** (2018), no. 16 163001, [[1801.04268](#)].
- [35] A. Nishizawa et al., *Laser-interferometric Detectors for Gravitational Wave Background at 100 MHz: Detector Design and Sensitivity*, *Phys. Rev. D* **77** (2008) 022002, [[0710.1944](#)].
- [36] L. P. Grishchuk, *Electromagnetic generators and detectors of gravitational waves*, in *1st Conference on High Frequency Gravitational Waves*, 6, 2003. [gr-qc/0306013](#).
- [37] V. B. Braginsky and V. N. Rudenko, *Gravitational Waves and the Detection of Gravitational Radiation*, *Phys. Rept.* **46** (1978) 165–200.

- [38] A. Ito, T. Ikeda, K. Miuchi, and J. Soda, *Probing GHz gravitational waves with graviton–magnon resonance*, *Eur. Phys. J. C* **80** (2020), no. 3 179, [[1903.04843](#)].
- [39] A. Ito and J. Soda, *A formalism for magnon gravitational wave detectors*, *Eur. Phys. J. C* **80** (2020), no. 6 545, [[2004.04646](#)].
- [40] Y. Kahn, J. Schütte-Engel, and T. Trickle, *Searching for High Frequency Gravitational Waves with Phonons*, [2311.17147](#).
- [41] G. Raffelt and L. Stodolsky, *Mixing of the Photon with Low Mass Particles*, *Phys. Rev. D* **37** (1988) 1237.
- [42] D. Boccaletti, V. De Sabbata, P. Fortini, and C. Gualdi, *Conversion of photons into gravitons and vice versa in a static electromagnetic field*, *Nuovo Cim. B* **70** (1970), no. 2 129–146.
- [43] A. Ringwald, J. Schütte-Engel, and C. Tamarit, *Gravitational Waves as a Big Bang Thermometer*, *JCAP* **03** (2021) 054, [[2011.04731](#)].
- [44] A. Ejlli, D. Ejlli, A. M. Cruise, G. Pisano, and H. Grote, *Upper limits on the amplitude of ultra-high-frequency gravitational waves from graviton to photon conversion*, *Eur. Phys. J. C* **79** (2019), no. 12 1032, [[1908.00232](#)].
- [45] A. Berlin, D. Blas, R. Tito D’Agnolo, S. A. R. Ellis, R. Harnik, et al., *Detecting high-frequency gravitational waves with microwave cavities*, *Phys. Rev. D* **105** (2022), no. 11 116011, [[2112.11465](#)].
- [46] V. Domcke, C. Garcia-Cely, and N. L. Rodd, *Novel Search for High-Frequency Gravitational Waves with Low-Mass Axion Haloscopes*, *Phys. Rev. Lett.* **129** (2022), no. 4 041101, [[2202.00695](#)].
- [47] M. E. Tobar, C. A. Thomson, W. M. Campbell, A. Quiskamp, J. F. Bourhill, et al., *Comparing Instrument Spectral Sensitivity of Dissimilar Electromagnetic Haloscopes to Axion Dark Matter and High Frequency Gravitational Waves*, *Symmetry* **14** (2022), no. 10 2165, [[2209.03004](#)].
- [48] A. D. Dolgov and D. Ejlli, *Conversion of relic gravitational waves into photons in cosmological magnetic fields*, *JCAP* **12** (2012) 003, [[1211.0500](#)].
- [49] V. Domcke and C. Garcia-Cely, *Potential of radio telescopes as high-frequency gravitational wave detectors*, *Phys. Rev. Lett.* **126** (2021), no. 2 021104, [[2006.01161](#)].
- [50] T. Liu, J. Ren, and C. Zhang, *Detecting High-Frequency Gravitational Waves in Planetary Magnetosphere*, [2305.01832](#).
- [51] A. Ito, K. Kohri, and K. Nakayama, *Probing high frequency gravitational waves with pulsars*, [2305.13984](#).
- [52] S. Ramazanov, R. Samanta, G. Trenkler, and F. R. Urban, *Shimmering gravitons in the gamma-ray sky*, *JCAP* **06** (2023) 019, [[2304.11222](#)].
- [53] A. Ito, K. Kohri, and K. Nakayama, *Gravitational wave search through electromagnetic telescopes*, [2309.14765](#).
- [54] C.-A. Faucher-Giguere and V. M. Kaspi, *Birth and evolution of isolated radio pulsars*, *Astrophys. J.* **643** (2006) 332–355, [[astro-ph/0512585](#)].
- [55] S. B. Popov, J. A. Pons, J. A. Miralles, P. A. Boldin, and B. Posselt, *Population synthesis studies of isolated neutron stars with magnetic field decay*, *Mon. Not. Roy. Astron. Soc.* **401** (2010) 2675–2686, [[0910.2190](#)].

- [56] E. O. Ofek, *Space and velocity distributions of Galactic isolated old Neutron stars*, *Publ. Astron. Soc. Pac.* **121** (2009) 814, [[0910.3684](#)].
- [57] N. Sartore, E. Ripamonti, A. Treves, and R. Turolla, *Galactic neutron stars I. Space and velocity distributions in the disk and in the halo*, *Astron. Astrophys.* **510** (2010) A23, [[0908.3182](#)].
- [58] B. R. Safdi, Z. Sun, and A. Y. Chen, *Detecting Axion Dark Matter with Radio Lines from Neutron Star Populations*, *Phys. Rev. D* **99** (2019), no. 12 123021, [[1811.01020](#)].
- [59] R. Hill, K. W. Masui, and D. Scott, *The Spectrum of the Universe*, *Appl. Spectrosc.* **72** (2018), no. 5 663–688, [[1802.03694](#)].
- [60] D. Ejlli and V. R. Thandlam, *Graviton-photon mixing*, *Phys. Rev. D* **99** (2019), no. 4 044022, [[1807.00171](#)].
- [61] D. Ejlli, *On the CMB circular polarization: I. The Cotton–Mouton effect*, *Eur. Phys. J. C* **79** (2019), no. 3 231, [[1810.04947](#)].
- [62] P. Chen, *Resonant photon - graviton conversion and cosmic microwave background fluctuations*, *Phys. Rev. Lett.* **74** (1995) 634–637. [Erratum: *Phys.Rev.Lett.* 74, 3091 (1995)].
- [63] P. Goldreich and W. H. Julian, *Pulsar electrodynamics*, *Astrophys. J.* **157** (1969) 869.
- [64] M. Maggiore, *Stochastic backgrounds of gravitational waves*, *ICTP Lect. Notes Ser.* **3** (2001) 397–414, [[gr-qc/0008027](#)].
- [65] R. N. Manchester et al., *The Parkes Multibeam Pulsar Survey. 1. Observing and data analysis systems, discovery and timing of 100 pulsars*, *Mon. Not. Roy. Astron. Soc.* **328** (2001) 17, [[astro-ph/0106522](#)].
- [66] R. T. Edwards, M. Bailes, W. van Straten, and M. C. Britton, *The Swinburne Intermediate Latitude Pulsar Survey*, *Mon. Not. Roy. Astron. Soc.* **326** (2001) 358, [[astro-ph/0105126](#)].
- [67] R. H. Cyburt, B. D. Fields, K. A. Olive, and T.-H. Yeh, *Big Bang Nucleosynthesis: 2015*, *Rev. Mod. Phys.* **88** (2016) 015004, [[1505.01076](#)].
- [68] V. Domcke, *Electromagnetic high-frequency gravitational wave detection*, in *57th Rencontres de Moriond on Electroweak Interactions and Unified Theories*, 6, 2023. [2306.04496](#).
- [69] G. F. Giudice, M. McCullough, and A. Urbano, *Hunting for dark particles with gravitational waves*, *Journal of Cosmology and Astroparticle Physics* **2016** (oct, 2016) 001.
- [70] M. Maggiore, *Gravitational Waves: Volume 1: Theory and Experiments*. Oxford University Press, 10, 2007.
- [71] G. Franciolini, A. Maharana, and F. Muia, *Hunt for light primordial black hole dark matter with ultrahigh-frequency gravitational waves*, *Phys. Rev. D* **106** (2022), no. 10 103520, [[2205.02153](#)].
- [72] A. Spitkovsky, *Time-dependent force-free pulsar magnetospheres: axisymmetric and oblique rotators*, *Astrophys. J. Lett.* **648** (2006) L51–L54, [[astro-ph/0603147](#)].
- [73] A. Philippov, A. Tchekhovskoy, and J. G. Li, *Time evolution of pulsar obliquity angle from 3D simulations of magnetospheres*, *Mon. Not. Roy. Astron. Soc.* **441** (2014), no. 3 1879–1887, [[1311.1513](#)].
- [74] S. Johnston and A. Karastergiou, *Pulsar braking and the $P-\dot{P}$ diagram*, *Mon. Not. Roy. Astron. Soc.* **467** (2017), no. 3 3493–3499, [[1702.03616](#)].

- [75] B. Zhang, A. K. Harding, and A. G. Muslimov, *Radio pulsar death line revisited: Is PSR J2144-3933 anomalous?*, *Astrophys. J. Lett.* **531** (2000) L135–L138, [[astro-ph/0001341](#)].
- [76] D. Bhattacharya, R. A. M. J. Wijers, J. W. Hartman, and F. Verbunt, *On the decay of the magnetic fields of single radio pulsars*, .
- [77] P. Goldreich and A. Reisenegger, *Magnetic Field Decay in Isolated Neutron Stars*, *Astrophysical Journal* **395** (Aug., 1992) 250.
- [78] D. A. Shalybkov and V. A. Urpin, *Ambipolar diffusion and anisotropy of resistivity in neutron star cores*, *Monthly Notices of the RAS* **273** (Apr., 1995) 643–648.
- [79] P. Haensel, V. A. Urpin, and D. G. Yakovlev, *Ohmic decay of internal magnetic fields in neutron stars*, *Astronomy and Astrophysics* **229** (Mar., 1990) 133–137.
- [80] W. D. Arnett, D. N. Schramm, and J. W. Truran, *On Relative Supernova Rates and Nucleosynthesis Roles*, *Astrophysical Journal, Letters* **339** (Apr., 1989) L25.
- [81] H. J. Rocha-Pinto, J. Scalo, W. J. Maciel, and C. Flynn, *Chemical enrichment and star formation in the Milky Way disk. II. Star formation history*, *Astronomy and Astrophysics* **358** (June, 2000) 869–885, [[astro-ph/0001383](#)].
- [82] S. K. Ballero, F. Matteucci, L. Origlia, and R. M. Rich, *Formation and evolution of the Galactic bulge: constraints from stellar abundances*, *Astronomy and Astrophysics* **467** (May, 2007) 123–136, [[astro-ph/0702137](#)].
- [83] D. R. Lorimer et al., *The Parkes multibeam pulsar survey: VI. Discovery and timing of 142 pulsars and a Galactic population analysis*, *Mon. Not. Roy. Astron. Soc.* **372** (2006) 777–800, [[astro-ph/0607640](#)].
- [84] R. T. Bartels, T. D. P. Edwards, and C. Weniger, *Bayesian model comparison and analysis of the Galactic disc population of gamma-ray millisecond pulsars*, *Mon. Not. Roy. Astron. Soc.* **481** (2018), no. 3 3966–3987, [[1805.11097](#)].
- [85] C. A. Faucher-Giguere and A. Loeb, *The Pulsar Contribution to the Gamma-Ray Background*, *JCAP* **01** (2010) 005, [[0904.3102](#)].
- [86] T. D. P. Edwards, B. J. Kavanagh, L. Visinelli, and C. Weniger, *Transient Radio Signatures from Neutron Star Encounters with QCD Axion Miniclusters*, *Phys. Rev. Lett.* **127** (2021), no. 13 131103, [[2011.05378](#)].
- [87] J. Binney, O. Gerhard, and D. Spergel, *The photometric structure of the inner galaxy*, *Mon. Not. Roy. Astron. Soc.* **288** (1997) 365–374, [[astro-ph/9609066](#)].
- [88] N. Bissantz and O. Gerhard, *Spiral arms, bar shape and bulge microlensing in the milky way*, *Mon. Not. Roy. Astron. Soc.* **330** (2002) 591, [[astro-ph/0110368](#)].